ADVANCING EARTH AND SPACE SCIENCE

Geophysical Research Letters

RESEARCH LETTER
10.1029/2022GL101987

Deep Long-Period Earthquakes at Akutan Volcano From 2005 to 2017 Better Track Magma Influxes Compared to Volcano-Tectonic Earthquakes

Zilin Song[1], Yen Joe Tan[1], and Diana C. Roman[2]

[1]Earth and Environmental Sciences Programme, Faculty of Science, The Chinese University of Hong Kong, Hong Kong, China, [2]Earth and Planets Laboratory, Carnegie Institution for Science, Washington, DC, USA

Key Points:

- Moment release rates of deep long-period events correlate more strongly with inflation episodes compared to volcano-tectonic events
- Akutan deep long-period earthquakes are likely due to non-stationary source effects like unsteady magma transport through complex pathways
- Akutan volcano-tectonic earthquakes represent fault ruptures triggered by magma/fluid movements or larger earthquakes

Supporting Information:

Supporting Information may be found in the online version of this article.

Correspondence to:

Y. J. Tan,
yjtan@cuhk.edu.hk

Citation:

Song, Z., Tan, Y. J., & Roman, D. C. (2023). Deep long-period earthquakes at Akutan Volcano from 2005 to 2017 better track magma influxes compared to volcano-tectonic earthquakes. *Geophysical Research Letters*, *50*, e2022GL101987. https://doi.org/10.1029/2022GL101987

Received 9 NOV 2022
Accepted 24 APR 2023

Abstract Both volcano-tectonic (VTs) and deep long-period earthquakes (DLPs) have been documented at Akutan Volcano, Alaska and may reflect different active processes helpful for eruption forecasting. In this study, we perform high-resolution earthquake detection, classification, and relocation using seismic data from 2005 to 2017 to investigate their relationship with underlying magmatic processes. We find that the 2,787 VTs and 787 DLPs are concentrated above and below the inferred magma reservoir respectively. They both are clustered as swarms and occur preferentially during inflation episodes with no spatial migrations. However, moment release rates of DLP swarms show a stronger correlation with inflation and their low-frequency content is likely a source instead of a path effect. Therefore, we infer that DLPs are directly related to unsteady magma movement through a complex pathway. In comparison, repeating events are observed in VTs. Thus, we conclude that they represent fault rupture triggered by magma/fluid movement or larger earthquakes.

Plain Language Summary Volcano eruption forecasting is a challenging task that often requires the deciphering of processes underlying observed signs of volcanic unrest. As seismometers become common monitoring sensors on volcanoes, the recorded ground motion is valuable for scientists to study eruption precursors. Earthquakes are commonly observed and generally inferred to be associated with stress perturbations in the shallow crust. However, earthquakes with predominantly lower-frequency energy are sometimes observed at depth and their origin is enigmatic. In this paper, we use the existing catalog of earthquakes at Akutan Volcano in Alaska between 2005 and 2017 as templates to successfully detect more earthquakes before locating them with higher precision. We find that earthquakes at Akutan Volcano tend to occur in swarms during times when the ground inflates due to magma accumulation beneath the volcano. Some earthquakes have predominantly low-frequency energy which suggests a different source mechanism compared to regular earthquakes. Furthermore, the largest events are more strongly correlated with surface inflation. Therefore, we conclude that these lower-frequency earthquakes are more directly related to unsteady magma movement through a complex pathway compared to regular earthquakes which represent fault rupture triggered by magma/fluid movement or larger earthquakes.

1. Introduction

Seismometers are the most commonly deployed monitoring sensors on volcanoes (Saccorotti & Lokmer, 2021) as exemplified by the seismic networks maintained by the Hawaiian (Nakata & Okubo, 2010) and Alaska (Power et al., 2013) volcano observatories. Over the years, development in volcano seismology has given rise to several successes in eruption forecasting. Precursory increases in seismicity rate are detected sometimes before major eruptions (R. A. White & McCausland, 2019), such as 1991 Pinatubo (Harlow et al., 1996), 2000 Hekla (Einarsson, 2018), and 2004 Mount St. Helens (Morgan et al., 2008) eruptions. However, seismic anomalies prior to eruptions are not always observed, limiting our forecasting ability. For instance, only 30% of recent eruptions among Alaskan volcanoes have statistically significant precursory increase in seismicity rate (Pesicek et al., 2018). Cameron et al. (2018) also found that between 1989 and 2017, Alaska Volcano Observatory's (AVO) forecasting success rate for certain types of volcanoes for example, those with short repose time (<15 years) or small eruption size (Volcanic Explosivity Index of 2 or less) is <20%. Therefore, further advances in our understanding of how seismic activity evolves through eruption cycles and relate to various volcanic and magmatic processes at different volcanoes are crucial for improving our ability to forecast eruptions (Thelen et al., 2022).

Earthquake occurrence is often clustered in space and time. The most common clustering is mainshock-aftershock sequences where the largest magnitude earthquake (i.e., mainshock) is followed by decaying numbers of smaller earthquakes nearby (i.e., aftershocks), with the magnitude difference between the mainshock and the largest aftershock being ~1.2 on average (Båth, 1965). Mainshock-aftershock sequences are generally thought to reflect a cascade of inter-event stress triggering (Marsan & Lengliné, 2008). Another type of clustering, where a burst of seismic activity is not associated with a clear mainshock, is described as swarm activity (Mogi, 1963; Roland & McGuire, 2009). Swarms occurring on plate boundary fault systems are often inferred to indicate fluid diffusion in heterogeneous structures (Nishikawa & Ide, 2017; Ross & Cochran, 2021) or aseismic slip in low coupling regions (Peng et al., 2021; Tan & Marsan, 2020). In comparison, swarms in volcanic or geothermal regions are often inferred to be related to migration of magma (Hensch et al., 2008; Power et al., 1998; Wilding et al., 2022) or hydrothermal fluids (Shelly et al., 2013), though these interpretations can be non-unique. In addition, while the proportion of swarms versus mainshock-aftershock sequences is thought to be higher in volcanic compared to non-volcanic regions (Benoit & McNutt, 1996), this is still under debate (Garza-Giron et al., 2018; Traversa & Grasso, 2010; Vidale et al., 2006). Therefore, it remains challenging to interpret the physical mechanism underlying bursts of seismic activity at volcanic regions.

Earthquakes recorded at volcanic regions that are rich in high-frequency content are usually referred to as volcano-tectonic events (VTs). VTs are commonly observed in the crust (e.g., Matoza et al. (2014)) and are considered to be related to stress perturbation from processes such as shear failures in volcanic edifice (B. A. Chouet & Matoza, 2013) or dike propagation (Roman & Cashman, 2006). In contrast, long-period earthquakes (LPs) radiate low-frequency (1–5 Hz) energy predominantly and have been detected in the shallow crust down to the upper mantle (Melnik et al., 2020; Pitt et al., 2002; R. A. White, 1996). Characterized by emergent phase arrivals and dominant low-frequency contents, LPs are difficult to detect using traditional earthquake detection methods (Pitt et al., 2002; Shapiro et al., 2017; Wimez & Frank, 2022), though recently, matched-filter detection techniques have proven to be quite effective for improving existing LP catalogs (Hotovec-Ellis et al., 2018; Kurihara & Obara, 2021; Kurihara et al., 2019). LPs occurring in the shallow crust have been attributed to pressure disruptions in the magmatic and hydrothermal systems (B. Chouet, 1992; Lokmer et al., 2008; Matoza & Roman, 2022; Matoza et al., 2015) or slow rupture in unconsolidated materials (Bean et al., 2014). In comparison, the inferred source mechanisms of LPs occurring from mid-crust to upper mantle (Kurihara & Obara, 2021; Power et al., 2004), known as deep long-period events (DLPs), is quite diverse but generally fall into two categories: (a) DLPs are generated near stalled magma for example, due to thermal stress from magma cooling (Aso & Tsai, 2014) or volatile release from second boiling (Wech et al., 2020); (b) DLPs are generated where there is unsteady fluid movement for example, due to intermittent magma flow (Ukawa & Ohtake, 1987), melt degassing (Melnik et al., 2020) or resonance in fluid-filled cracks (B. A. Chouet, 1996; B. A. Chouet & Matoza, 2013). Since DLPs could provide a crucial window into the deep plumbing system and are potential eruption precursors (Power et al., 2013; R. A. White, 1996), identifying the specific processes underlying DLPs will improve our ability to interpret unrest episodes and forecast eruptions. However, while VTs' utility for eruption forecasting is well-studied (Li et al., 2021; R. White & McCausland, 2016), our understanding of how DLP activity might relate differently to inflation and eruption episodes remains limited.

Akutan Volcano is one of the most active volcanoes in the Aleutian Arc with at least 27 eruptive episodes reported since 1790 (Lu & Dzurisin, 2014; Miller et al., 1998). Seismometers have been deployed at Akutan volcano since 1996 forming a network of 14 stations at present with which both VTs and DLPs are documented (Power et al., 2004). In addition, based on both Interferometric Synthetic Aperture Radar (InSAR) (Lu et al., 2000; Wang et al., 2018) and local Global Positioning System (GPS) (Ji & Herring, 2011; Ji et al., 2017) observations, a magma reservoir is inferred to be located at ~8 km depth with inflation episodes observed every 2–3 years between 2002 and 2017. Therefore, Akutan Volcano is a promising site to investigate the characteristics of DLPs and VTs and their relationship to magmatic processes. In this paper, we analyze 12 years of continuous waveform data at Akutan Volcano to detect and locate VTs and DLPs using cross-correlation-based template matching (Gibbons & Ringdal, 2006) and double-difference relocation (Waldhauser & Ellsworth, 2000). We then characterize their spatiotemporal clustering properties and how their activities relate with the inflation episodes, as well as investigate the underlying cause for the waveform characteristics of DLPs.

2. Matched Filter Detection, Magnitude Estimation, and Relocation

Between November 2005 and December 2017, continuous waveform data from 14 stations (Figure 1a) are available from the Incorporated Research Institution for Seismology Data Management Center (IRIS DMC), whereas

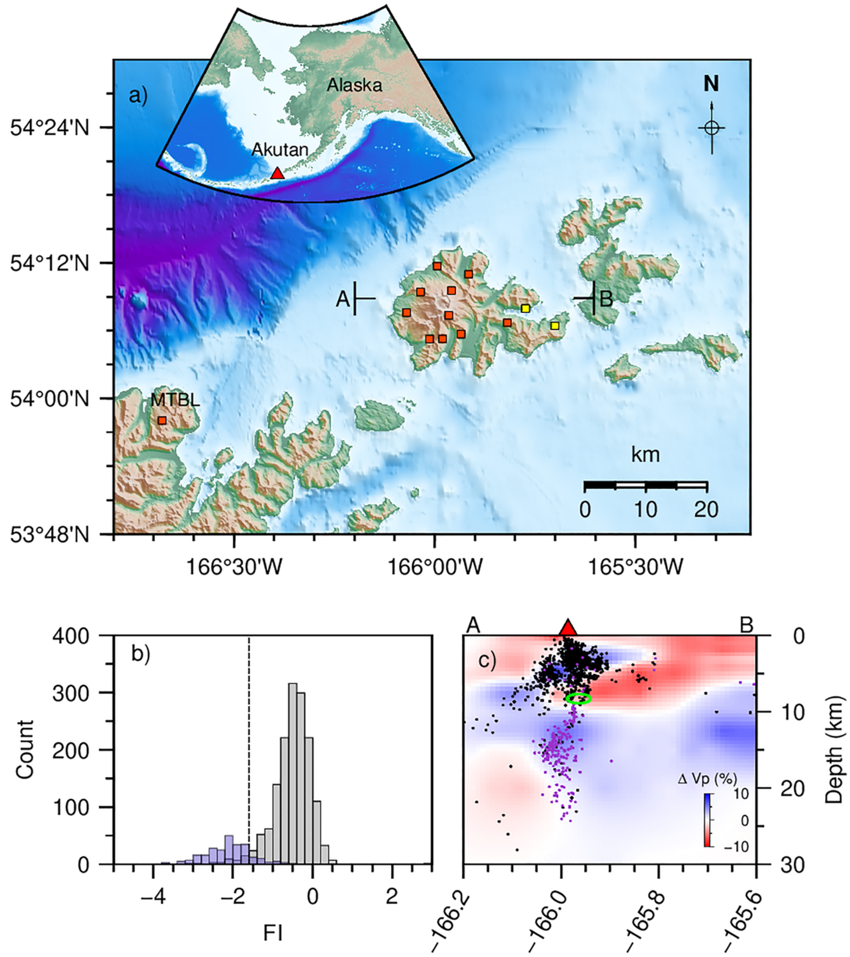

Figure 1. Map view of Akutan Volcano along with earthquake distribution. (a) Topography of Akutan Island with cross section from A to B shown in panel (c) Squares represent seismometers used in this study with yellow squares highlighting sites with two co-located seismometers. The inset shows the location of Akutan Volcano in Alaska. (b) Frequency index (FI) distribution for 2002–2017 earthquakes with dashed line indicating the threshold of −1.6 used to separate different earthquake types in our study. Colors represent different labels assigned by analysts, that is, light gray represents VTs while purple represents LPs. (c) *P* wave velocity anomalies across Akutan Volcano (Syracuse et al., 2015) overlain by relocated seismicity during 2005–2017. Earthquakes classified as VTs and LPs using FI are represented by black and purple dots respectively. Green ellipse marks the deformation source estimated by DeGrandpre et al. (2017).

between 2002 and 2005, 1-min event waveforms are available (Alaska Volcano Observatory/USGS, 1988). Therefore, we obtain waveforms of 1,785 events from 2002 to 2017 in the unified catalog of earthquakes produced by the AVO (Power et al., 2019) falling in the study region (Figure 1). All waveforms are resampled to 50 Hz and bandpass filtered at 1–15 Hz.

We apply EQcorrscan, an open-source python package, to perform matched filter detection (Chamberlain et al., 2017). By cross-correlating waveforms of template events with continuous waveforms across the seismic network, detections are declared when the sum of normalized cross-correlations (NCC) exceeds a certain threshold. We use 1,510 events recorded by four stations, where the signal-to-noise ratio of *P* arrival on the vertical channel and *S* arrival on the horizontal channel is above 2, as templates. Template waveforms start from 1 s before *P*/*S* arrivals and have lengths of 7 s. Each template is used to scan through continuous data from 2005 to 2017 (Figure S1 in Supporting Information S1). To improve the stability of the detection process, we split the continuous waveforms into hourly segments with 30 s overlaps and remove traces with excessive gaps or spikes before the template matching process (Warren-Smith et al., 2017).

We use 10 times median absolute deviation (MAD) as a conservative threshold for declaring a detection following Hotovec-Ellis et al. (2018). Since the matched filter detection method mainly detects events with similar waveforms as the templates, our detections can be limited by the available initial catalog of templates. To quantify this effect, we check whether each of our 1,278 templates between 2005 and 2017 is detected from continuous waveforms by any other templates using EQcorrscan. We find that 99.6% of the templates are successfully detected by another template which suggests that the method can detect unique events reasonably well. We further manually inspect new detections' waveforms and remove detections with average network NCC that is less than 0.4 to remove false detections. Finally, for detections with origin time difference of less than 2 s, the ones with the lowest NCC values are removed to avoid duplicates (van Wijk et al., 2021). We end up with 2,077 newly-detected events.

For newly-detected events, we estimate their local magnitudes as follow:

$$M_{detection} = M_{template} + c * \log(\alpha) \tag{1}$$

where α is the amplitude ratio between detected and template events while c is a constant that scales the amplitude-magnitude difference and is approximately 1 (Figure S2 in Supporting Information S1) (Schaff, 2008; Shelly et al., 2016). We measure α using principal component analysis on 7 s long waveforms and use the median α value from paired waveforms across all the available stations. The magnitude of completeness (M_c) is improved from M_L 0.1 to M_L −0.3 (Figure S3 in Supporting Information S1) when estimated using the maximum curvature method (Wiemer & Wyss, 2000).

We then relocate both the catalog (Power et al., 2019) and newly detected events using the HypoDD double-difference method (Waldhauser & Ellsworth, 2000). Newly detected events are assumed to be co-located with their templates as initial input to HypoDD. We calculate pick-derived differential arrival times for all event pairs within 10 km of each other with at least six observations. For event pairs with distance less than 5 km, we derive cross-correlation-derived differential arrival times at each station when NCC value of the waveforms is larger than 0.7. The window begins 0.5 s before and continue for 1.5 and 2 s after the P and S-wave arrivals, respectively. We successfully relocate 3,144 events using a 3D velocity model from Syracuse et al. (2015) between November 2005 and December 2017 (Figure 1c). We then perform bootstrapping by repeatedly relocating 100 random events using singular value decomposition mode to estimate their location uncertainties (Waldhauser & Ellsworth, 2000). On average, we find that the relative horizontal and vertical location uncertainties are 0.75 and 1.07 km, respectively.

3. Earthquake Classification

The long-period (LP) and VT events in the AVO catalog have been manually classified (Power et al., 2019), but manual classifications are subjective and can be inconsistent (Matoza et al., 2014). Therefore, we reclassify all events systematically using the frequency index (FI) following Buurman and West (2010) and Matoza et al. (2014):

$$FI = \log_{10}\left(\overline{A}_{upper}/\overline{A}_{lower}\right) \tag{2}$$

where $\overline{A}_{upper}$ and $\overline{A}_{lower}$ represent mean spectral amplitudes in the higher and lower frequency bands respectively. For each event, we calculate the power spectral density spectrum of its vertical component seismograms with a 7 s time window starting from 1 s before the P picks, after correcting for instrument response. When P pick is unavailable from the catalog, we use the predicted arrival time derived from the event location and 1-D velocity model (Power et al., 2019). We first calculate FI at each station using 10–15 Hz and 1–5 Hz as the A_{upper} and A_{lower}, respectively, since we find that these frequency bands allow the FI to most effectively differentiate the VTs and DLPs (Figure S4 in Supporting Information S1). The median FI across all available stations is then assigned to each event as their final FI value (Matoza et al., 2014).

Figure 1b shows the FI distribution of earthquakes in the AVO catalog, color-coded by their manual labels (Power et al., 2019). There is a clear bimodal distribution and near the boundary, manual labels can be inconsistent that is, events with the same FI values can have different labels. We select FI of −1.6 as the classification boundary, hence 259 events with FI lower than −1.6 are classified as LP while the remaining events are classified as VT. Newly detected events are classified into the same category as their templates. Overall, 561 newly detected events are LPs which is 2 times more than the number of LP templates. In comparison, 1,516 newly detected events are

10.1029/2022GL101987

VTs which is similar to the number of VT templates. The larger number of new detection relative to the available templates for LP events may reflect AVO's current event detection system being less well-optimized for detecting LP events.

Combined with earthquake spatial distributions (Figure 1c), we observe that (a) most VTs are located beneath the caldera and above the inferred magma reservoir (DeGrandpre et al., 2017); (b) there are some VTs located to the west of the caldera that extend down to 30 km depth; (c) most LPs are located below the inferred magma reservoir in a region with low P wave velocity (Syracuse et al., 2015). We refer to these LPs below the inferred magma reservoir as DLPs.

4. Earthquake Clusters and Moment Release

We cluster the LP and VT events above M_c separately following Mogi (1963)'s algorithm which takes into account (a) the total number of events in a sequence (E_T), and (b) the empirical relation between maximum number of daily events (N_d) and duration of sequence in days (T):

$$N_d > 2 \times \sqrt{T} \tag{3}$$

E_T of 5, 10, and 15 are applied separately as the minimum threshold to see which criteria works best. We then iterate through T values from 0.5 to 5 to ensure both short- and long-duration clusters can be identified. For each cluster, we calculate the distance between each clustered earthquake and the largest one. Events located further than three times standard deviation from the largest earthquake are regarded as outliers and removed. To improve clustering results, absolute locations are also used for earthquakes that are not successfully relocated (Figure S5 in Supporting Information S1). After manually checking the magnitude-time evolution of each cluster given by different E_T thresholds, we decide to focus on clusters identified by E_T of 10 in the following discussion while those given by E_T of 5 and 15 will be used to evaluate the robustness of our conclusions. For $E_T \geq 10$, 8 DLP and 34 VT clusters (Figure 2c) are identified and further classified as swarms when (a) the magnitude difference between the largest magnitude event and the following second largest events in one cluster is less than 1, and (b) the occurrence time of the largest event in one cluster is near/after the middle of the sequence. We find that all DLP and VT clusters fulfill these criteria and are classified as swarms (Figure S6 in Supporting Information S1). There are no mainshock-aftershock sequences detected no matter which E_T we choose (Figure S7 in Supporting Information S1).

For each swarm, we estimate its cumulative moment release. The seismic moment (M_0) of each event is calculated as

$$M_0 = 10^{1.5*M_w+9.105} \tag{4}$$

where M_w represents an earthquake's moment magnitude. We obtain each event's M_w by converting their M_L following $M_w = M_L$ for $M_L > 3$ events (Kanamori & Brodsky, 2004) and $M_w = 2/3*M_L + 1$ for $M_L \leq 3$ events (Munafò et al., 2016), which accounts for the expected change in scaling between M_L and M_w for smaller earthquakes (Deichmann, 2017). Cumulative moment release of a swarm is the sum of M_0 for all the involved earthquakes.

5. Discussion

5.1. Dominant Frequency Content of DLPs

As the VTs and DLPs predominantly are located in different regions (Figure 1c), the difference in their dominant frequency content could be a result of differences in wave propagation path with different attenuation effects. First, we investigate whether the lower frequency content of DLPs can be a path effect due to the overlying low velocity regions (Figure S8a in Supporting Information S1) with the presence of melt or extensive fracturing (Clarke et al., 2021; Coté et al., 2010). We calculate the FI values of DLPs recorded at the MTBL station which is located ~50 km west of Akutan Volcano (Figure 1a). We find that their FI values remain low (Figure 3a) and similar to the FI values measured using waveforms recorded on the local stations (Figure 1b). In comparison, deep VTs located a few kilometers west of the DLP zone recorded on the MTBL station all have higher FI values (Figures 3a and 3b) despite having similar travel paths (Figure S8a in Supporting Information S1). Therefore, we conclude that the lower frequency content of DLPs at Akutan Volcano is not only a path effect due to the overlying structure.

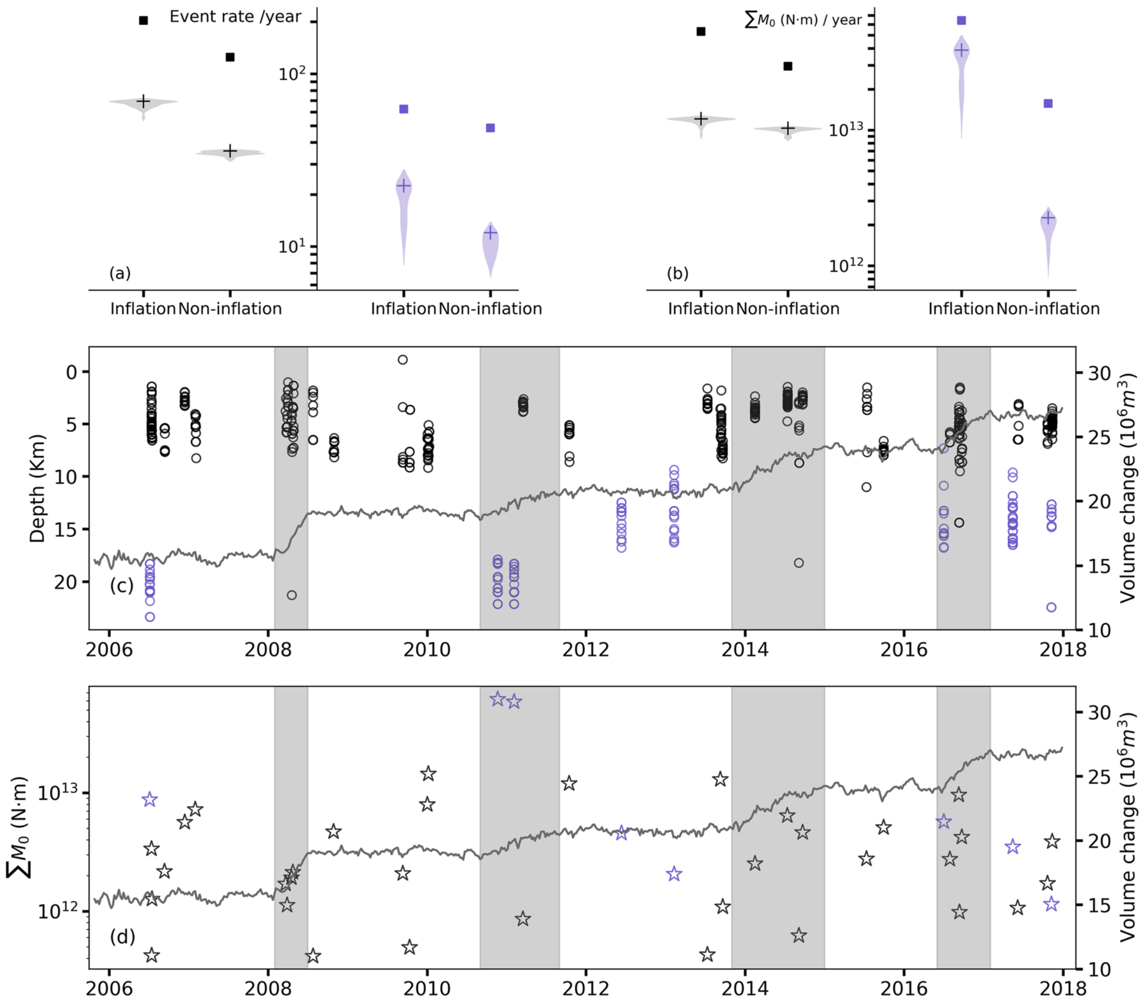

Figure 2. Properties of earthquakes at Akutan Volcano from 2005 to 2017. Event rates (a) and moment release rates (b) of deep long-period earthquakes (DLPs) (purple) and volcano-tectonic earthquakes (VTs) (black) during inflation and non-inflation periods. The violin plots show results of Jack-knife test where we leave one swarm out and recalculate properties iteratively. The violin widths are scaled by data counts. Cross symbols and squares indicate properties of clustered earthquakes and all earthquakes, respectively. (c) Temporal evolution of earthquake depths. Purple and black circles represent DLP and VT swarms, respectively. Gray curve represents volume changes of deformation source as calculated by Xue et al. (2020). Shaded areas mark inflation episodes. (d) Cumulative moment release of earthquake swarms. Purple and black stars indicate DLP and VT swarms, respectively.

Subsequently, we investigate whether the lower frequency content of DLPs is a path effect due to attenuation in their source region (Figure S8b in Supporting Information S1). In this case, there should not be any VT events in the DLP source region. However, while they do not occur in large numbers, we manage to identify ~60 deep VT events within the DLP source region (Figures 3b and 3c, Figure S9 in Supporting Information S1). Time differences between P and S arrivals of the deep VTs are similar to those of deep LPs and significantly larger than those of shallow VTs, indicating that these deep VTs are not mislocated (Figure 3c, Figure S9 in Supporting Information S1). Hence, the lower frequency content of DLPs at Akutan Volcano is unlikely to be only a path effect due to attenuation in their source region. Therefore, we conclude that the lower frequency content of DLPs at Akutan Volcano is most probably a source effect, though we cannot completely rule out the possibility of kilometer-scale structural heterogeneity with highly variable attenuation effect around the DLP source region (Figure S8c in Supporting Information S1).

5.2. How VT and DLP Swarms Relate to Inflation Episodes

Earthquake swarms have been found to sometimes coincide with surface deformation driven by high-pressure fluid or magma injection, for example, Green and Neuberg (2006), Ji et al. (2017), and Shelly et al. (2013), or aseismic slip propagation, for example, Gualandi et al. (2017) and Yukutake et al. (2022). However, few studies

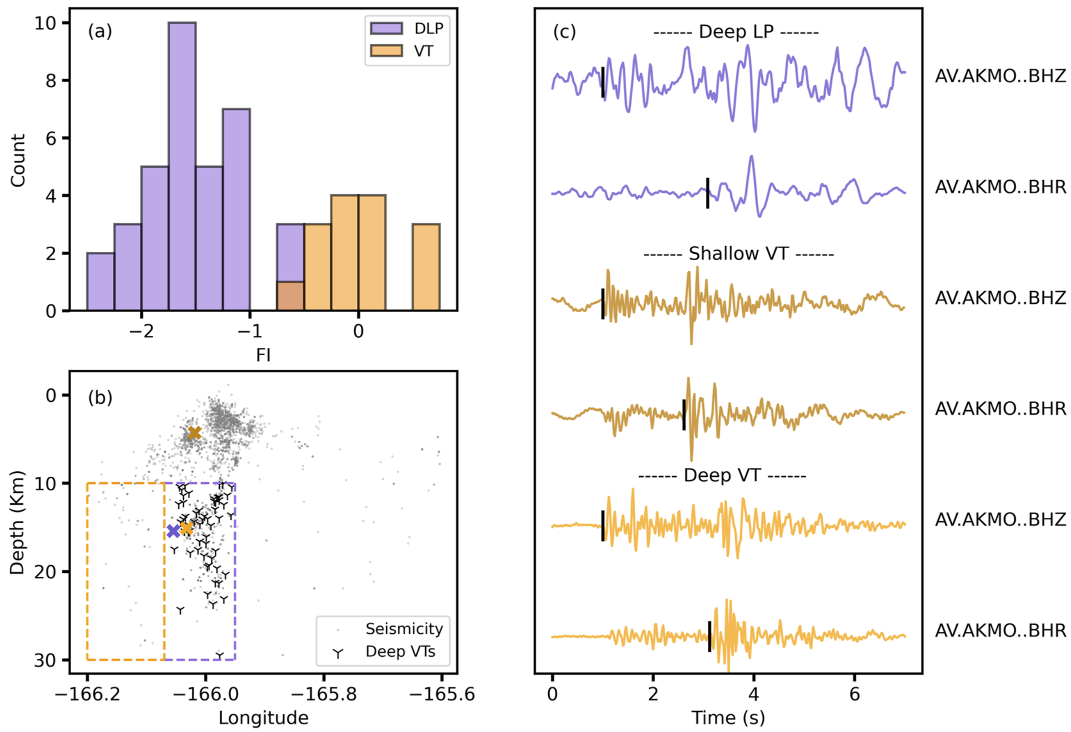

Figure 3. Frequency index analysis on deep volcano-tectonic (VTs) and deep long-period earthquakes (DLPs). (a) Frequency index measured at station MTBL (Figure 1a) for DLPs and deep VTs to the west of the caldera, with their spatial boundaries outlined by purple and yellow boxes, respectively in panel (b). (b) Seismicity distribution during 2005–2017 are shown by gray dots. VT detections within the DLP source region are marked as black trident scatters. Purple, light yellow, and dark yellow crosses show locations of DLP, deep VT and shallow VT shown in panel (c); (c) Representative waveforms of DLP (purple), deep (light yellow) and shallow (dark yellow) VTs recorded by the same local station at vertical and radial channels. Black vertical lines indicate phase arrivals.

have quantified how VT and DLP swarms might behave differently over decadal timescales and in relation to differently with various magmatic processes. Such an analysis could help us better decipher swarms' underlying physical processes and utility for eruption forecasting. Therefore, we analyze temporal correlations between identified swarms and surface deformation at Akutan Volcano. Based on GPS measurement from November 2005 to December 2017, we manually identify four inflation episodes, each lasting 5–14 months (Figures 2c and 2d), when the inferred Mogi source exhibits a significant volume increase (Xue et al., 2020). In total, the inflation episodes span 39 months out of the 145 months that our study period encompasses.

We find that 3 (73 DLPs) out of the 8 DLP swarms (179 DLPs) and 13 (225 VTs) out of the 34 VT swarms (541 VTs) occurred during inflation episodes. This means that the rate of DLP and VT swarms are 0.92 and 4.00 per year (22.46 DLPs/year and 69.23 VTs/year), respectively during the inflating periods, which is almost twice the rate of 0.57 and 2.38 per year (12.00 DLPs/year and 35.77 VTs/year) during the non-inflating periods (Figure 2a). This finding is relatively robust, since we find that both DLP and VT swarms rates during inflating episodes remain higher than during non-inflating periods even when we do not cluster earthquakes (Figure 2a) or use minimum E_T of 5 or 15 instead during the clustering process (Figure S10 in Supporting Information S1). We also applied Jack-knife test by iteratively recalculating all these statistics after dropping out one cluster at a time to evaluate whether our observed trend could be a by-product of overwhelming influence from any individual swarm. The Jack-knife test results show the range of event rate for both DLP and VT swarms in inflating periods remains higher than non-inflating periods (Figure 2a), indicating that our conclusion is not biased by any individual swarm. Both DLP and VT occurrences are strongly correlated with magma inflation.

Previous research suggests that cumulative moment release of proximal volcanic earthquake swarms in a single swarm can be used as a proxy for intruded magma volume (Kettlety et al., 2022). If this relationship holds for Akutan Volcano, swarms occurring during inflation episodes should have larger cumulative moment releases compared to those occurring during non-inflation periods. We find that the two largest DLP swarms in terms of cumulative moment releases indeed occurred during an inflation episode (Figure 2d). The third DLP swarm that occurred during an inflation episode in 2016 had comparable cumulative moment releases with the two largest DLP swarms that occurred during non-inflation periods. In comparison, the largest VT swarms in terms of cumulative moment releases do not coincide with inflation episodes (Figure 2d). We also estimate the moment release rates of DLP and VT swarms during inflation and non-inflation periods (Figure 2b). We find that the moment release rates of DLP swarms during inflation periods is 3.88×10^{13} N · m/year, which is 15 times larger than 2.26×10^{12} N · m/year during non-inflation periods. Comparatively, the moment release rates of VT swarms in inflation periods (1.21×10^{13} N · m/year) is only 17% higher than that in non-inflation periods (1.03×10^{13} N · m/year). This pattern remains consistent when we do not cluster events (Figure 2b), or use E_T of 5 and 15 instead during the clustering process (Figure S10 in Supporting Information S1). The Jack-knife test results also show the same trend (Figure 2b) which means that this conclusion is not biased by any individual swarm including when clustering parameter changes (Figure S10 in Supporting Information S1). Therefore, it appears that compared to VT swarms, the moment release of DLP swarms is more strongly correlated with magma inflation. Interestingly, the two largest DLP swarms occurred during the 2011 inflation period which has relatively slower inflation rate than other inflation episodes (Figure 2d). This is similar to observations at Sierra Negra Volcano (Bell et al., 2021) and Santorini Volcano (Druitt et al., 2019) where seismic moment release rates do not always correlate with inflation rates. Possible explanations include the seismic moment release being only a fraction of the moment release of the deformation (Gualandi et al., 2017), and is also affected by factors such as the stress state of the region (Pedersen et al., 2007).

5.3. Physical Process Underlying VT and DLP Swarms

VT swarms are commonly inferred to be related to physical processes like dike propagation (Roman & Cashman, 2006), fluid diffusion (Yukutake et al., 2011), and aseismic slip (Yukutake et al., 2022) based on observations of vertical alignment in earthquake distributions (Roman & Cashman, 2006), earthquake migration speed that gives reasonable diffusivity/permeability estimates (Yukutake et al., 2011), and detections of repeating earthquakes (Yukutake et al., 2022). In comparison, DLP swarms have been associated with magma transport based on their low-frequency energy content, non-double-couple source moment tensor (Oikawa et al., 2019), and migration path that co-locates with estimated magma movement path (Kurihara et al., 2019) or stalled magma at depth based on observations of stationary, repeating DLPs that correlate with gas emissions (Wech et al., 2020). At Akutan Volcano, we discover that all the clustered VTs and DLPs are swarms instead of mainshock-aftershock sequences with none of them delineating planar structures or showing spatial migration from depth with time (Figure 2c, Figure S6 in Supporting Information S1). Such event migrations should have been resolvable since half of all identified swarms span at least 5 km spatially. Unlike observations at Mammoth mountains (Power et al., 1998), Long Valley caldera (Li et al., 2021), and Fagradalsfjall eruption (Fischer et al., 2022) where migrating seismicities can be used to track magma movements as dike propagates, the absence of migrating seismicity at Akutan Volcano is comparable to swarms detected at Makushin Volcano in 2020 (Lanza et al., 2022). Therefore, we conclude that seismic swarms at Akutan are unlikely to represent dike propagation.

Interestingly, VT swarms at Akutan Volcano are mostly located within regions with high V_p (Figure 1c) interpreted as regions with low fluid content (Yukutake et al., 2015). However, due to the limited spatial resolution of the tomography study (Syracuse et al., 2015), it remains possible that these swarms are triggered by small-scale fluid diffusion (Hatch et al., 2020; Igarashi et al., 2003). In addition, we have identified "repeating" events with highly similar (NCC > 0.9) waveforms (Figure S11 in Supporting Information S1) within these swarms, though we could not verify that their rupture areas indeed overlap. Considering that the VT swarms are more likely to occur during inflation episodes with no spatial migration, they might reflect fault asperities that were driven to failure due to stress loading from the underlying inflating magma reservoir. However, since many VT swarms, including the ones with the largest cumulative moment release, occur during non-inflation periods, they are likely also linked to other non-magmatic processes for example, fluid diffusion (Farrell et al., 2009) or triggering by nearby or far-field large earthquakes (Peng et al., 2021).

Repeating DLPs are usually interpreted to reflect a repeating, non-destructive source process occurring at the same location, such as rapid pressure changes due to magmatic gas passing through cracks at Fuego volcano (Brill & Waite, 2019) or resonance of a fixed geometry fluid-filled crack at Mauna Loa Volcano (Okubo &

Wolfe, 2008). Previous studies have also attributed volcanic LPs to slow fault ruptures (Bean et al., 2014), which are similar to repeating LPs observed in non-volcanic environments such as the Japan subduction zone plate interface (Nishikawa et al., 2019). However, out of the ~600 DLPs at Akutan Volcano, we only find one pair with NCC value above 0.9 and these two events have FI of −1.7 which is close to the boundary of −1.6 that we used to separate LP and VT events. Therefore, we conclude that DLPs at Akutan Volcano do not reflect either a stationary, repeating source process or slow fault ruptures. Instead, since they are clustered as swarms without spatial migration, correlated with inflation episodes, located just beneath the inferred magma reservoir, and have low-frequency content likely due to source effect, we infer that DLPs at Akutan Volcano are directly related to unsteady magma movement through a complex pathway (Kurihara et al., 2019). In this case, the lack of DLP swarms during certain inflation episodes (Figure 2b) could reflect aseismic magma movement, that is, magma flow that do not radiate detectable seismic energy (Gualandi et al., 2017). DLP swarms occurring outside of inflation episodes with smaller cumulative moment release (Figure 2c) could instead represent magma influxes that do not generate detectable surface deformation signal for the existing GPS network.

6. Conclusions

In conclusion, we detect 2,077 new events at Akutan Volcano by applying template matching on continuous data from 2005 to 2017. We then systematically classify all events into 2,787 VTs and 767 LPs based on their FI. After waveform-based double difference relocation, we find that the VTs and DLPs are primarily distributed above and below the inferred magma reservoir respectively. The low-frequency content of DLPs is relatively uniform across the seismic network, thus is likely a source instead of only path or site effect. After clustering both VTs and DLPs based on their interevent time, distance and magnitude, we find that they both only occur as swarms instead of mainshock-aftershock sequences. In addition, while they occur asynchronously with no clear spatial migration, both DLP and VT swarms occur preferentially during inflation episodes. However, the largest DLP swarms (in terms of cumulative moment release) coincide well with inflation episodes whereas the largest VT swarms occur during non-inflation periods. Furthermore, repeating events are only detected in VTs and not in DLPs. Therefore, we infer that compared to VT swarms that likely reflect fault slips triggered by magma inflation, fluid diffusion or larger earthquakes, DLP swarms are more directly related to unsteady magma movement through a complex pathway.

Data Availability Statement

A unified catalog of earthquake hypocenters and magnitudes at Alaska volcanoes during 1989–2018 from Power et al. (2019) is used for this research, which is available at https://doi.org/10.3133/sir20195037. Using IRIS Data Services, waveforms and related metadata from Alaska Volcano Observatory and Alaska Regional Network can be accessed at https://doi.org/10.7914/SN/AK and https://doi.org/10.7914/SN/AV.

Acknowledgments
This work is supported by the Direct Grant for Research (Grant 4053512) from the Chinese University of Hong Kong, Hong Kong RGC General Research Fund (Grant 14300422), and the Croucher Tak Wah Mak Innovation Award. We would like to thank editor Christian Huber, reviewer Robin Matoza and an anonymous reviewer for constructive comments that helped improve the manuscript significantly.

References

Alaska Volcano Observatory/USGS. (1988). Alaska Volcano Observatory. International federation of digital seismograph networks. Retrieved from https://www.fdsn.org/networks/detail/AV/

Aso, N., & Tsai, V. C. (2014). Cooling magma model for deep volcanic long-period earthquakes. *Journal of Geophysical Research: Solid Earth*, *119*(11), 8442–8456. https://doi.org/10.1002/2014JB011180

Båth, M. (1965). Lateral inhomogeneities of the upper mantle. *Tectonophysics*, *2*(6), 483–514. https://doi.org/10.1016/0040-1951(65)90003-x

Bean, C. J., De Barros, L., Lokmer, I., Métaxian, J.-P., O' Brien, G., & Murphy, S. (2014). Long-period seismicity in the shallow volcanic edifice formed from slow-rupture earthquakes. *Nature Geoscience*, *7*(1), 71–75. https://doi.org/10.1038/ngeo2027

Bell, A. F., Hernandez, S., La Femina, P. C., & Ruiz, M. C. (2021). Uplift and seismicity driven by magmatic inflation at Sierra Negra Volcano, Galápagos Islands. *Journal of Geophysical Research: Solid Earth*, *126*(7), e2021JB022244. https://doi.org/10.1029/2021JB022244

Benoit, J. P., & McNutt, S. R. (1996). Global volcanic earthquake swarm database 1979-1989. (Report No. 96-69). Retrieved from http://pubs.er.usgs.gov/publication/ofr9669

Brill, K. A., & Waite, G. P. (2019). Characteristics of repeating long-period seismic events at Fuego Volcano, January 2012. *Journal of Geophysical Research: Solid Earth*, *124*(8), 8644–8659. https://doi.org/10.1029/2019JB017902

Buurman, H., & West, M. (2010). *Seismic precursors to volcanic explosions during the 2006 eruption of Augustine Volcano*. The 2006 Eruption of Augustine Volcano. 1769

Cameron, C. E., Prejean, S. G., Coombs, M. L., Wallace, K. L., Power, J. A., & Roman, D. C. (2018). Alaska Volcano Observatory alert and forecasting timeliness: 1989–2017. *Frontiers of Earth Science*, *6*, 86. https://doi.org/10.3389/feart.2018.00086

Chamberlain, C. J., Hopp, C. J., Boese, C. M., Warren-Smith, E., Chambers, D., Chu, S. X., et al. (2017). Eqcorrscan: Repeating and near-repeating earthquake detection and analysis in python. *Seismological Research Letters*, *89*(1), 173–181. https://doi.org/10.1785/0220170151

Chouet, B. (1992). A seismic model for the source of long-period events and harmonic tremor. In *Volcanic seismology* (pp. 133–156). Springer.

Chouet, B. A. (1996). Long-period volcano seismicity: Its source and use in eruption forecasting. *Nature*, *380*(6572), 309–316. https://doi.org/10.1038/380309a0

Chouet, B. A., & Matoza, R. S. (2013). A multi-decadal view of seismic methods for detecting precursors of magma movement and eruption. *Journal of Volcanology and Geothermal Research*, *252*, 108–175. https://doi.org/10.1016/j.jvolgeores.2012.11.013

Clarke, J., Adam, L., & van Wijk, K. (2021). LP or VT signals? How intrinsic attenuation influences volcano seismic signatures constrained by whakaari volcano parameters. *Journal of Volcanology and Geothermal Research*, *418*, 107337. https://doi.org/10.1016/j.jvolgeores.2021.107337

Coté, D. M., Belachew, M., Quillen, A. C., Ebinger, C. J., Keir, D., Ayele, A., & Wright, T. (2010). Low-frequency hybrid earthquakes near a magma chamber in Afar: Quantifying path effects. *Bulletin of the Seismological Society of America*, *100*(5A), 1892–1903. https://doi.org/10.1785/0120090111

DeGrandpre, K., Wang, T., Lu, Z., & Freymueller, J. T. (2017). Episodic inflation and complex surface deformation of Akutan Volcano, Alaska revealed from GPS time-series. *Journal of Volcanology and Geothermal Research*, *347*, 337–359. https://doi.org/10.1016/j.jvolgeores.2017.10.003

Deichmann, N. (2017). Theoretical basis for the observed break in m_l/m_w scaling between small and large earthquakes. *Bulletin of the Seismological Society of America*, *107*(2), 505–520. https://doi.org/10.1785/0120160318

Druitt, T. H., Pyle, D. M., & Mather, T. A. (2019). Santorini volcano and its plumbing system. *Elements*, *15*(3), 177–184. https://doi.org/10.2138/gselements.15.3.177

Einarsson, P. (2018). Short-term seismic precursors to Icelandic eruptions 1973–2014. *Frontiers of Earth Science*, *6*, 45. https://doi.org/10.3389/feart.2018.00045

Farrell, J., Husen, S., & Smith, R. B. (2009). Earthquake swarm and b-value characterization of the Yellowstone volcano-tectonic system. *Journal of Volcanology and Geothermal Research*, *188*(1), 260–276. https://doi.org/10.1016/j.jvolgeores.2009.08.008

Fischer, T., Hrubcová, P., Salama, A., Doubravová, J., Ágústsdóttir, T., Gudnason, E., et al. (2022). Swarm seismicity illuminates stress transfer prior to the 2021 Fagradalsfjall eruption in Iceland. *Earth and Planetary Science Letters*, *594*, 117685. https://doi.org/10.1016/j.epsl.2022.117685

Garza-Giron, R., Brodsky, E. E., & Prejean, S. G. (2018). Mainshock-aftershock clustering in volcanic regions. *Geophysical Research Letters*, *45*(3), 1370–1378. https://doi.org/10.1002/2017GL075738

Gibbons, S. J., & Ringdal, F. (2006). The detection of low magnitude seismic events using array-based waveform correlation. *Geophysical Journal International*, *165*(1), 149–166. https://doi.org/10.1111/j.1365-246X.2006.02865.x

Green, D. N., & Neuberg, J. (2006). Waveform classification of volcanic low-frequency earthquake swarms and its implication at Soufrière Hills Volcano, Montserrat. *Journal of Volcanology and Geothermal Research*, *153*(1), 51–63. https://doi.org/10.1016/j.jvolgeores.2005.08.003

Gualandi, A., Nichele, C., Serpelloni, E., Chiaraluce, L., Anderlini, L., Latorre, D., et al. (2017). Aseismic deformation associated with an earthquake swarm in the northern Apennines (Italy). *Geophysical Research Letters*, *44*(15), 7706–7714. https://doi.org/10.1002/2017GL073687

Harlow, D. H., Power, J. A., Laguerta, E. P., Ambubuyog, G., White, R. A., & Hoblitt, R. P. (1996). Precursory seismicity and forecasting of the June 15, 1991, eruption of Mount Pinatubo. *Fire and Mud: eruptions and lahars of Mount Pinatubo, Philippines* (pp. 223–247).

Hatch, R. L., Abercrombie, R. E., Ruhl, C. J., & Smith, K. D. (2020). Evidence of aseismic and fluid-driven processes in a small complex seismic swarm near Virginia city, Nevada. *Geophysical Research Letters*, *47*(4), e2019GL085477. https://doi.org/10.1029/2019GL085477

Hensch, M., Riedel, C., Reinhardt, J., & Dahm, T. (2008). Hypocenter migration of fluid-induced earthquake swarms in the Tjörnes Fracture Zone (North Iceland). *Tectonophysics*, *447*(1), 80–94. https://doi.org/10.1016/j.tecto.2006.07.015

Hotovec-Ellis, A. J., Shelly, D. R., Hill, D. P., Pitt, A. M., Dawson, P. B., & Chouet, B. A. (2018). Deep fluid pathways beneath Mammoth mountain, California, illuminated by migrating earthquake swarms. *Science Advances*, *4*(8), eaat5258. https://doi.org/10.1126/sciadv.aat5258

Igarashi, T., Matsuzawa, T., & Hasegawa, A. (2003). Repeating earthquakes and interplate aseismic slip in the northeastern Japan subduction zone. *Journal of Geophysical Research*, *108*(B5), 2249. https://doi.org/10.1029/2002JB001920

Ji, K. H., & Herring, T. A. (2011). Transient signal detection using GPS measurements: Transient inflation at Akutan Volcano, Alaska, during early 2008. *Geophysical Research Letters*, *38*(6), L06307. https://doi.org/10.1029/2011gl046904

Ji, K. H., Yun, S.-H., & Rim, H. (2017). Episodic inflation events at Akutan Volcano, Alaska, during 2005–2017. *Geophysical Research Letters*, *44*(16), 8268–8275. https://doi.org/10.1002/2017gl074626

Kanamori, H., & Brodsky, E. E. (2004). The physics of earthquakes. *Reports on Progress in Physics*, *67*(8), 1429–1496. https://doi.org/10.1088/0034-4885/67/8/r03

Kettlety, T., Kendall, J. M., & Roman, D. C. (2022). Self-similarity of seismic moment release to volume change scaling for volcanoes: A comparison with injection-induced seismicity. *Geophysical Research Letters*, *49*(23), e2022GL099369. https://doi.org/10.1029/2022GL099369

Kurihara, R., & Obara, K. (2021). Spatiotemporal characteristics of relocated deep low-frequency earthquakes beneath 52 volcanic regions in Japan over an analysis period of 14 years and 9 months. *Journal of Geophysical Research: Solid Earth*, *126*(10), e2021JB022173. https://doi.org/10.1029/2021JB022173

Kurihara, R., Obara, K., Takeo, A., & Tanaka, Y. (2019). Deep low-frequency earthquakes associated with the eruptions of Shinmoe-dake in KirishimaVolcanoes. *Journal of Geophysical Research: Solid Earth*, *124*(12), 13079–13095. https://doi.org/10.1029/2019JB018032

Lanza, F., Roman, D. C., Power, J. A., Thurber, C. H., & Hudson, T. (2022). Complex magmatic-tectonic interactions during the 2020 Makushin Volcano, Alaska, earthquake swarm. *Earth and Planetary Science Letters*, *587*, 117538. https://doi.org/10.1016/j.epsl.2022.117538

Li, B. Q., Smith, J. D., & Ross, Z. E. (2021). Basal nucleation and the prevalence of ascending swarms in long valley caldera. *Science Advances*, *7*(35), eabi8368. https://doi.org/10.1126/sciadv.abi8368

Lokmer, I., Saccorotti, G., Di Lieto, B., & Bean, C. J. (2008). Temporal evolution of long-period seismicity at Etna Volcano, Italy, and its relationships with the 2004–2005 eruption. *Earth and Planetary Science Letters*, *266*(1), 205–220. https://doi.org/10.1016/j.epsl.2007.11.017

Lu, Z., & Dzurisin, D. (2014). Insar imaging of aleutian volcanoes. In *Insar imaging of aleutian volcanoes* (pp. 87–345). Springer.

Lu, Z., Wicks, C., Power, J. A., & Dzurisin, D. (2000). Ground deformation associated with the March 1996 earthquake swarm at Akutan Volcano, Alaska, revealed by satellite radar interferometry. *Journal of Geophysical Research*, *105*(B9), 21483–21495. https://doi.org/10.1029/2000jb900200

Marsan, D., & Lengliné, O. (2008). Extending earthquakes' reach through cascading. *Science*, *319*(5866), 1076–1079. https://doi.org/10.1126/science.1148783

Matoza, R. S., Chouet, B. A., Dawson, P. B., Shearer, P. M., Haney, M. M., Waite, G. P., et al. (2015). Source mechanism of small long-period events at Mount St. Helens in July 2005 using template matching, phase-weighted stacking, and full-waveform inversion. *Journal of Geophysical Research: Solid Earth*, *120*(9), 6351–6364. https://doi.org/10.1002/2015JB012279

Matoza, R. S., & Roman, D. C. (2022). One hundred years of advances in volcano seismology and acoustics. *Bulletin of Volcanology*, *84*(9), 86. https://doi.org/10.1007/s00445-022-01586-0

Matoza, R. S., Shearer, P. M., & Okubo, P. G. (2014). High-precision relocation of long-period events beneath the summit region of Kılauea Volcano, Hawai'i, from 1986 to 2009. *Geophysical Research Letters*, *41*(10), 3413–3421. https://doi.org/10.1002/2014gl059819

Melnik, O., Lyakhovsky, V., Shapiro, N. M., Galina, N., & Bergal-Kuvikas, O. (2020). Deep long period volcanic earthquakes generated by degassing of volatile-rich basaltic magmas. *Nature Communications*, *11*(1), 3918. https://doi.org/10.1038/s41467-020-17759-4

Miller, T. P., McGimsey, R., Richter, D., Riehle, J., Nye, C., Yount, M., & Dumoulin, J. A. (1998). *Catalog of the historically active volcanoes of Alaska*. United States Department of the Interior, United States Geological Survey.

Mogi, K. (1963). Some discussions on aftershocks, foreshocks and earthquake swarms: The fracture of a semi-infinite body caused by an inner stress origin and its relation to the earthquake phenomena (third paper). *Bulletin of the Earthquake Research Institute, University of Tokyo*, *41*(3), 615–658.

Morgan, S. C., Malone, S. D., Qamar, A. I., Thelen, W. A., Wright, A. K., & Caplan-Auerbach, J. (2008). Seismicity associated with renewed dome building at Mount st. Helens, 2004–2005. (Report No. 1750-2). Retrieved from http://pubs.er.usgs.gov/publication/pp17502

Munafò, I., Malagnini, L., & Chiaraluce, L. (2016). On the relationship between m_w and m_l for small earthquakes. *Bulletin of the Seismological Society of America*, *106*(5), 2402–2408. https://doi.org/10.1785/0120160130

Nakata, J. S., & Okubo, P. G. (2010). *Hawaiian volcano observatory seismic data, January–March 2009*. US Geological Survey Open-File Report. 1079.

Nishikawa, T., & Ide, S. (2017). Detection of earthquake swarms at subduction zones globally: Insights into tectonic controls on swarm activity. *Journal of Geophysical Research: Solid Earth*, *122*(7), 5325–5343. https://doi.org/10.1002/2017JB014188

Nishikawa, T., Matsuzawa, T., Ohta, K., Uchida, N., Nishimura, T., & Ide, S. (2019). The slow earthquake spectrum in the Japan trench illuminated by the s-net seafloor observatories. *Science*, *365*(6455), 808–813. https://doi.org/10.1126/science.aax5618

Oikawa, G., Aso, N., & Nakajima, J. (2019). Focal mechanisms of deep low-frequency earthquakes beneath Zao Volcano, northeast Japan, and relationship to the 2011 Tohoku earthquake. *Geophysical Research Letters*, *46*(13), 7361–7370. https://doi.org/10.1029/2019GL082577

Okubo, P. G., & Wolfe, C. J. (2008). Swarms of similar long-period earthquakes in the mantle beneath Mauna Loa Volcano. *Journal of Volcanology and Geothermal Research*, *178*(4), 787–794. https://doi.org/10.1016/j.jvolgeores.2008.09.007

Pedersen, R., Sigmundsson, F., & Einarsson, P. (2007). Controlling factors on earthquake swarms associated with magmatic intrusions; constraints from Iceland. *Journal of Volcanology and Geothermal Research*, *162*(1), 73–80. https://doi.org/10.1016/j.jvolgeores.2006.12.010

Peng, W., Marsan, D., Chen, K. H., & Pathier, E. (2021). Earthquake swarms in Taiwan: A composite declustering method for detection and their spatial characteristics. *Earth and Planetary Science Letters*, *574*, 117160. https://doi.org/10.1016/j.epsl.2021.117160

Pesicek, J. D., Wellik, J. J., Prejean, S. G., & Ogburn, S. E. (2018). Prevalence of seismic rate anomalies preceding volcanic eruptions in Alaska. *Frontiers of Earth Science*, *6*(100). https://doi.org/10.3389/feart.2018.00100

Pitt, A., Hill, D., Walter, S., & Johnson, M. (2002). Midcrustal, long-period earthquakes beneath northern California volcanic areas.

Power, J. A., Friberg, P. A., Haney, M. M., Parker, T., Stihler, S. D., & Dixon, J. P. (2019). A unified catalog of earthquake hypocenters and magnitudes at volcanoes in Alaska—1989–2018. (Report No. 2019-5037). Retrieved from http://pubs.er.usgs.gov/publication/sir20195037

Power, J. A., Stihler, S. D., Chouet, B. A., Haney, M. M., & Ketner, D. M. (2013). Seismic observations of redoubt volcano, Alaska—1989–2010 and a conceptual model of the redoubt magmatic system. *Journal of Volcanology and Geothermal Research*, *259*, 31–44. https://doi.org/10.1016/j.jvolgeores.2012.09.014

Power, J. A., Stihler, S. D., White, R. A., & Moran, S. C. (2004). Observations of deep long-period (DLP) seismic events beneath Aleutian arc volcanoes; 1989–2002. *Journal of Volcanology and Geothermal Research*, *138*(3–4), 243–266. https://doi.org/10.1016/j.jvolgeores.2004.07.005

Power, J. A., Villaseñor, A., & Benz, H. M. (1998). Seismic image of the mount spurr magmatic system. *Bulletin of Volcanology*, *60*(1), 27–37. https://doi.org/10.1007/s004450050214

Roland, E., & McGuire, J. J. (2009). Earthquake swarms on transform faults. *Geophysical Journal International*, *178*(3), 1677–1690. https://doi.org/10.1111/j.1365-246X.2009.04214.x

Roman, D. C., & Cashman, K. V. (2006). The origin of volcano-tectonic earthquake swarms. *Geology*, *34*(6), 457–460. https://doi.org/10.1130/g22269.1

Ross, Z. E., & Cochran, E. S. (2021). Evidence for latent crustal fluid injection transients in southern California from long-duration earthquake swarms. *Geophysical Research Letters*, *48*(12), e2021GL092465. https://doi.org/10.1029/2021GL092465

Saccorotti, G., & Lokmer, I. (2021). Chapter 2—A review of seismic methods for monitoring and understanding active volcanoes. In P. Papale (Ed.), *Forecasting and planning for volcanic hazards, risks, and disasters* (Vol. 2, pp. 25–73). Elsevier. Retrieved from https://www.sciencedirect.com/science/article/pii/B9780128180822000020

Schaff, D. P. (2008). Semiempirical statistics of correlation-detector performance. *Bulletin of the Seismological Society of America*, *98*(3), 1495–1507. https://doi.org/10.1785/0120060263

Shapiro, N. M., Droznin, D. V., Droznina, S. Y., Senyukov, S. L., Gusev, A. A., & Gordeev, E. I. (2017). Deep and shallow long-period volcanic seismicity linked by fluid-pressure transfer. *Nature Geoscience*, *10*(6), 442–445. https://doi.org/10.1038/ngeo2952

Shelly, D. R., Ellsworth, W. L., & Hill, D. P. (2016). Fluid-faulting evolution in high definition: Connecting fault structure and frequency-magnitude variations during the 2014 Long Valley caldera, California, earthquake swarm. *Journal of Geophysical Research: Solid Earth*, *121*(3), 1776–1795. https://doi.org/10.1002/2015JB012719

Shelly, D. R., Hill, D. P., Massin, F., Farrell, J., Smith, R. B., & Taira, T. (2013). A fluid-driven earthquake swarm on the margin of the Yellowstone caldera. *Journal of Geophysical Research: Solid Earth*, *118*(9), 4872–4886. https://doi.org/10.1002/jgrb.50362

Syracuse, E. M., Maceira, M., Zhang, H., & Thurber, C. H. (2015). Seismicity and structure of Akutan and Makushin volcanoes, Alaska, using joint body and surface wave tomography. *Journal of Geophysical Research: Solid Earth*, *120*(2), 1036–1052. https://doi.org/10.1002/2014jb011616

Tan, Y. J., & Marsan, D. (2020). Connecting a broad spectrum of transient slip on the San Andreas fault. *Science Advances*, *6*(33), eabb2489. https://doi.org/10.1126/sciadv.abb2489

Thelen, W. A., Matoza, R. S., & Hotovec-Ellis, A. J. (2022). Trends in volcano seismology: 2010 to 2020 and beyond. *Bulletin of Volcanology*, *84*(3), 26. https://doi.org/10.1007/s00445-022-01530-2

Traversa, P., & Grasso, J.-R. (2010). How is volcano seismicity different from tectonic seismicity? *Bulletin of the Seismological Society of America*, *100*(4), 1755–1769. https://doi.org/10.1785/0120090214

Ukawa, M., & Ohtake, M. (1987). A monochromatic earthquake suggesting deep-seated magmatic activity beneath the izu-ooshima volcano, Japan. *Journal of Geophysical Research*, *92*(B12), 12649–12663. https://doi.org/10.1029/jb092ib12p12649

van Wijk, K., Chamberlain, C. J., Lecocq, T., & Van Noten, K. (2021). Seismic monitoring of the Auckland volcanic field during New Zealand's covid-19 lockdown. *Solid Earth*, *12*(2), 363–373. https://doi.org/10.5194/se-12-363-2021

Vidale, J. E., Boyle, K. L., & Shearer, P. M. (2006). Crustal earthquake bursts in California and Japan: Their patterns and relation to volcanoes. *Geophysical Research Letters*, *33*(20), L20313. https://doi.org/10.1029/2006GL027723

Waldhauser, F., & Ellsworth, W. L. (2000). A double-difference earthquake location algorithm: Method and application to the northern hayward fault, California. *Bulletin of the Seismological Society of America*, *90*(6), 1353–1368. https://doi.org/10.1785/0120000006

Wang, T., DeGrandpre, K., Lu, Z., & Freymueller, J. T. (2018). Complex surface deformation of Akutan Volcano, Alaska revealed from inSAR time series. *International Journal of Applied Earth Observation and Geoinformation*, *64*, 171–180. https://doi.org/10.1016/j.jag.2017.09.001

Warren-Smith, E., Chamberlain, C. J., Lamb, S., & Townend, J. (2017). High-precision analysis of an aftershock sequence using matched-filter detection: The 4 May 2015 ML 6 Wanaka earthquake, Southern Alps, New Zealand. *Seismological Research Letters*, *88*(4), 1065–1077. https://doi.org/10.1785/0220170016

Wech, A. G., Thelen, W. A., & Thomas, A. M. (2020). Deep long-period earthquakes generated by second boiling beneath Mauna Kea Volcano. *Science*, *368*(6492), 775–779. https://doi.org/10.1126/science.aba4798

White, R., & McCausland, W. (2016). Volcano-tectonic earthquakes: A new tool for estimating intrusive volumes and forecasting eruptions. *Journal of Volcanology and Geothermal Research*, *309*, 139–155. https://doi.org/10.1016/j.jvolgeores.2015.10.020

White, R. A. (1996). Precursory deep long-period earthquakes at Mount Pinatubo: Spatio-temporal link to a basalt trigger. *Fire and mud: Eruptions and lahars of Mount Pinatubo, Philippines* (pp. 307–328).

White, R. A., & McCausland, W. A. (2019). A process-based model of pre-eruption seismicity patterns and its use for eruption forecasting at dormant stratovolcanoes. *Journal of Volcanology and Geothermal Research*, *382*, 267–297. https://doi.org/10.1016/j.jvolgeores.2019.03.004

Wiemer, S., & Wyss, M. (2000). Minimum magnitude of completeness in earthquake catalogs: Examples from Alaska, the Western United States, and Japan. *Bulletin of the Seismological Society of America*, *90*(4), 859–869. https://doi.org/10.1785/0119990114

Wilding, J. D., Zhu, W., Ross, Z. E., & Jackson, J. M. (2022). The magmatic web beneath hawai 'i. *Science*, *379*(6631), eade5755. https://doi.org/10.1126/science.ade5755

Wimez, M., & Frank, W. B. (2022). A recursive matched-filter to systematically explore volcanic long-period earthquake swarms. *Geophysical Journal International*, *231*(2), 912–920. https://doi.org/10.1093/gji/ggac221

Xue, X., Freymueller, J., & Lu, Z. (2020). Modeling the posteruptive deformation at okmok based on the GPS and inSAR time series: Changes in the shallow magma storage system. *Journal of Geophysical Research: Solid Earth*, *125*(2), e2019JB017801. https://doi.org/10.1029/2019jb017801

Yukutake, Y., Honda, R., Harada, M., Arai, R., & Matsubara, M. (2015). A magma-hydrothermal system beneath hakone volcano, central Japan, revealed by highly resolved velocity structures. *Journal of Geophysical Research: Solid Earth*, *120*(5), 3293–3308. https://doi.org/10.1002/2014JB011856

Yukutake, Y., Ito, H., Honda, R., Harada, M., Tanada, T., & Yoshida, A. (2011). Fluid-induced swarm earthquake sequence revealed by precisely determined hypocenters and focal mechanisms in the 2009 activity at Hakone Volcano, Japan. *Journal of Geophysical Research*, *116*(B4), B04308. https://doi.org/10.1029/2010JB008036

Yukutake, Y., Yoshida, K., & Honda, R. (2022). Interaction between aseismic slip and fluid invasion in earthquake swarms revealed by dense geodetic and seismic observations. *Journal of Geophysical Research: Solid Earth*, *127*(4), e2021JB022933. https://doi.org/10.1029/2021JB022933